J Nanopart Res (2012) 14:1137
DOI 10.1007/s11051-012-1137-5

RESEARCH PAPER

Cytotoxicity evaluation of nanoclays in human epithelial cell line A549 using high content screening and real-time impedance analysis

Navin K. Verma · Edward Moore · Werner Blau · Yuri Volkov · P. Ramesh Babu

Received: 21 September 2011 / Accepted: 14 August 2012 / Published online: 28 August 2012

Abstract Continuously expanding use of products containing nanoclays for wide range of applications have raised public concerns about health and safety. Although the products containing nanoclays may not be toxic, it is possible that nanomaterials may come in contact with humans during handling, manufacture, or disposal, and cause adverse health impact. This necessitates biocompatibility evaluation of the commonly used nanoclays. Here, we investigated the cytotoxic effects of platelet (Bentone MA, ME-100, Cloisite Na^+, Nanomer PGV, and Delite LVF) and tubular (Halloysite, and Halloysite MP1) type nanoclays on cultured human lung epithelial cells A549. For the first time with this aim, we employed a cell-based automated high content screening in combination with real-time impedance sensing. We demonstrate varying degree of dose- and time-dependent cytotoxic effects of both nanoclay types. Overall, platelet structured nanoclays were more cytotoxic than tubular type. A low but significant level of cytotoxicity was observed at 25 μg/mL of the platelet-type nanoclays. A549 cells exposed to high concentration (250 μg/mL) of tubular structured nanoclays showed inhibited cell growth. Confocal microscopy indicated intracellular accumulation of nanoclays with perinuclear localization. Results indicate a potential hazard of nanoclay-containing products at significantly higher concentrations, which warrant their further biohazard assessment on the actual exposure in humans.

Keywords Nanoclay · Cytotoxicity · High content screening · Impedance sensing

N. K. Verma · Y. Volkov
Department of Clinical Medicine, Institute of Molecular Medicine, Trinity College Dublin, Dublin 8, Ireland

N. K. Verma · Y. Volkov · P. Ramesh Babu (✉)
Centre for Research on Adaptive Nanostructures & Nanodevices, Trinity College Dublin, Dublin 2, Ireland
e-mail: babup@tcd.ie

E. Moore · W. Blau · P. Ramesh Babu
School of Physics, Trinity College Dublin, Dublin 2, Ireland

Introduction

Nanoclays are nano-sized natural materials originating from clay fraction of soil. They are receiving considerable attention in recent years because of their potential use in hundreds of commercial products as nanoscale inclusions, filler materials, and structural components. The attraction of exploiting nanoclays for various purposes is due to their high surface area and unique physicochemical properties. They are being incorporated into a wide variety of modern products including electronics, food, clothing, tyres, medicines, sunscreens, cosmetics, sporting equipment, polymer composites, bone implants, controlled drug delivery, protective coatings (e.g., anticorrosion, antibacterial, or antimolding), and for materials synthesis (Floody

et al. 2009). Nanoclay-enabled polymeric systems (e.g., plastic nanocomposites) are being developed to create unique devices for use in next-generation biological applications including antimicrobial agents, drug delivery, bioimaging probes, and cancer treatment (Suresh et al. 2010; Dong and Feng 2005; Lin et al. 2002; Nayak and Sahoo 2011). With this rapid development of nano-inspired research, new nanoscale materials including nanoclay particles might have unintended impacts on human health. These potential health and safety issues require more attention as the nanotechnology industry grows, and consequently more nanoscale wastes are released into the environment. Thus, in order to allow the safe and sustainable development of such nanomaterials or nanoenabled products, there is an immediate need for research to study their potential toxicity for practical applications and to address uncertainties about the health effects.

Nanoparticles range in aerodynamic size from 1 nm to 100 nm. They can escape air filters, contaminate ambient air, penetrate deep into the lungs, reach the alveolar region and evoke adverse pulmonary effects. In addition, it is increasingly being recognized that adverse health effects of nanomaterials depend on their specific characteristics including particle composition, size, shape, electrostatic charge, and related reactivity with biological systems (Oberdorster et al. 2005a, b; Powers et al. 2006; Napierska et al. 2010). Nano-size particles mainly enter our body via inhalation through a respiratory route and alveolar epithelial cells are the first line of defence that interact with the inhaled particles. In this study, we selected an immortalized human alveolar epithelial cell line A549 as a model system of airborne particle exposure. A549 cells have been well-characterized and widely used for comprehending pulmonary nanotoxicity (Stearns et al. 2001; Ahamed 2011). We analyzed possible toxic effects of commercially available nanoclays of various physical structures by utilizing ultrasensitive cytotoxicity detection methods based on high content image analysis and real-time impedance sensing.

Materials and methods

Nanoclays

Bentone MA was obtained from Elementis Specialities (NJ, USA), ME-100 was from Coop Chemicals (Tokyo, Japan), Cloisite Na^+ was from Southern Clay Products (TX, USA), Delilite LVF was from Laviosa Minerals S.p.A (Livorno, Italy), Nanomer PGV was from Nanocore (IL, USA), Halloysite was from Sigma-Aldrich (Wicklow, Ireland), and Halloysite MP1 was from Imerys Tableware (Auckland, New Zealand). To examine cellular uptake, Cloisite nanoclay was fluorescently labeled with Rhodamine by ion exchange reaction and the modified clay was washed thoroughly to remove un-reacted rhodamine dye.

Cell culture and treatments

Human alveolar epithelial cells (A549 cell line, ATCC, Manassas, VA, USA) were cultured as described (Mohamed et al. 2011). Briefly, cells were cultured in Ham's F12 medium supplemented with 10 % (v/v) fetal bovine serum, 10,000 U penicillin and 10 mg/mL streptomycin in 5 % CO_2 at 37 °C in a humidified incubator. For experimentation, cells were seeded in 96-well plates at the density of 5×10^3 cell/well and allowed to grow overnight prior to treatment. All the nanoclays were dispersed in cell culture medium prior to administration to the cells. Serial dilutions were established by mixing equal volumes of particle suspension and cell culture medium followed by vigorous vortexing, and applied to the cell immediately.

Zeta potential measurements

Zeta potential of the nanoclays was determined using the Malvern Instruments Zetasizer Nano ZS. The nanoclay powders were dispersed at a concentration of 50 mg/mL in Millipore water in a sonic bath and placed in clear disposable Zeta potential capillary cells. The measurements were carried out at 25 °C.

Scanning electron microscopy (SEM)

To examine the morphological structure of the nanoclays, a Zeiss supra scanning electron microscope was used. Samples were deposited onto conductive carbon tabs and covered with metallic gold to obtain adequate contrast of the structure.

Transmition electron microscopy (TEM)

To examine the nanoscale features of the nanoclays, a Joel 2100 transmission electron microscope was used.

The nanoclays were dispersed in Millipore water using a sonication process and a drop of each sample was deposited onto a carbon grid and allowed to dry in a fume hood overnight. The images were recorded digitally using an AMT digital camera.

Confocal microscopy

Cells were seeded in a 8-well Permanox® chamber slide (20×10^3 cells/well) and exposed to rhodamine labeled Cloisite for the time intervals indicated in the text and figure legends. After exposure, cells were washed with phosphate-buffered saline (PBS) and fixed in 3 % paraformaldehyde (15 min at room temperature). They were fluorescently counterstained with Alexa Fluor 488 phlloidin and Hoechst. Fluorescence confocal images were taken using Zeiss LSM510-Meta (Carl Zeiss Microimaging Inc., NY, USA) using 40× objective lens. At least 20 different microscopic fields were analyzed for each sample.

High content screening and analysis

High content screening protocols have been optimized and established in our laboratory as described (Mohamed et al. 2011). Briefly, A549 cells were seeded in 96-well plates (4×10^3 cells/well), exposed to various concentrations of nanoclays at 37 °C and 5 % CO_2, washed with PBS, and fixed in 3 % paraformaldehyde. Cells were fluorescently stained with Alexa Fluor 488 phalloidin to visualize the cellular morphology and Hoechst to visualize the nuclei. Plates were scanned (five randomly selected fields/well) using an automated microscope IN Cell Analyzer 1000 (GE Healthcare, UK). Quantitative estimations of the acquired images were performed with IN Cell Investigator software using multi-parameter cytotoxicity bio-application module (GE Healthcare, UK).

Real-time impedance sensing

Real-time monitoring of electrical impedance (which depends on cell number, degree of adhesion, spreading, and proliferation of the cells) to determine cytotoxic effects of nanoclays was performed using xCELLigance system as per manufacturer's instructions (Roche Applied Science, West Sussex, UK). Briefly, cells were seeded at a density of 5×10^3 cells/well into 100 µl of media in the E-Plate® (cross interdigitated micro-electrodes integrated on the bottom of 96-well tissue culture plates by micro-electronic sensor technology) and allowed to attach onto the electrode surface over time. The electrical impedance was recorded every 15 min. At 20-h time point, when cells adhered to the well properly, they were treated with nanoclays in triplicates and monitored for additional 76 h. The cell impedance, expressed as an arbitrary unit called the 'Cell Index', were automatically calculated on the xCELLigence system and converted into growth curves.

Statistical analysis

The data are expressed as mean ± SEM. For comparison of two groups, p values were calculated by two-tailed unpaired student's t test. In all cases, p values < 0.05 were considered to be statistically significant. Correlation coefficients were determined using Gretl statistical analysis software.

Results

Characterization of nanoclays

TEM and SEM images of Bentone MA (a representative platelet-type nanoclay) and Halloysite (a representative tubular-type nanoclay) are shown in Fig. 1. Table 1 summarizes important physicochemical properties of the nanoclays such as purity, specific surface area, zeta potential, etc., which are known to critically influence nanoparticle uptake and toxicity. The measured zeta potential, a parameter of particle diffusion degree, of individual nanoclays were in the range of −32 to −52 mV in the medium (Table 1). The high absolute value of the zeta potential ensures a stable suspension because of the strength of the electrostatic repulsion force.

Nanoclay uptake by A549 cells

Although the detail mechanisms of nanoclay uptake by lung epithelial cells do not serve the purpose of this study, we, however, performed cellular uptake analysis of Cloisite Na^+ as a representative example of the nanoclay of moderate toxicity characteristics. The fluorescent conjugates of nanoparticles serve as a marker to quantitatively determine their cellular

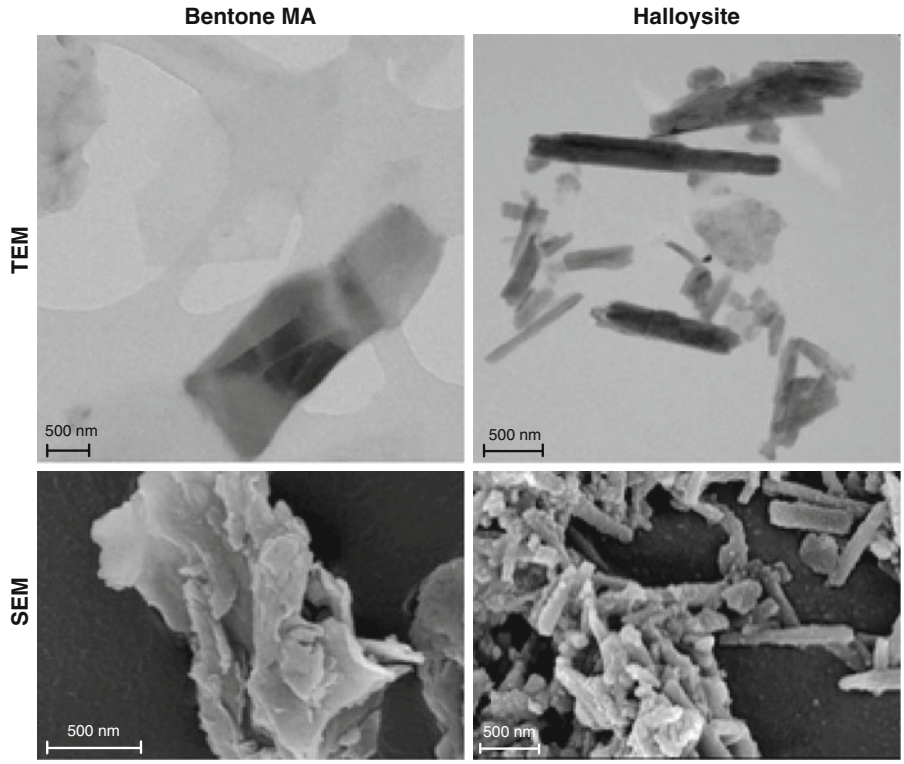

Fig. 1 Representative TEM and SEM images of tubular- and platelet-type nanoclays. Mean particle size of Bentone MA (platelet type) range from 91 to 302 nm (magnification, 350,000×) and that of Halloysite (tubular type) from 453 to 1112 nm (magnification, 40,000×)

Table 1 Physiochemical properties of the prepared nanoclays

Geometry	Nanoclays	Chemical formula	Purity (%)	Zeta potential (mV)	Specific surface area (m^2/g)
Tubular	Halloysite MP1	$Al_2Si_2O_5(OH)_4 \times 2H_20$	90	−41	65
	Halloysite	$Al_2Si_2O_5(OH)_4 \times 2H_2O$	90	−32.1	64
Platelet	Nanomer PGV	M^+ $y(Al_{2-y}$ $Mg_y)(Si_4)$ $O_{10}(OH)_2 \times nH_2O$	100	−51.9	ND
	ME-100	$Na_{2x}Mg_{3.0-x}Si_4O_{10}(F_yOH_{1-y})_2$	100	−52.3	9
	Delelite LVF	$(Si,Al)_8(Al,Fe,Mg)_4O_{20}(OH)_4$, Xn,m($H_2O$)	100	−45.1	600
	Bentone MA	$Na_{0.4}Mg_{2.7}Li_{0.3}Si_4O_{10}$ $(OH)_2$	98	−36.6	600
	Cloisite Na^+	$(Na,Ca)_{0.33}(Al,Mg)_2Si_4O_{10}(OH)_2$	98	−48.6	800

ND not tested

uptake and intracellular distribution. To examine whether nanoclays are able to enter lung epithelium, we incubated A549 cells with rhodamine-labeled Cloisite (25 μg/mL) for up to 24 h. Examination using a confocal fluorescent microscope showed internalized nanoclay particles in A549 cells. Strong fluorescent signals were detectable in treated cells but not in the control group indicating intracellular accumulation of Cloisite particles and/or agglomerates (Fig. 2). The accumulation of the particles/

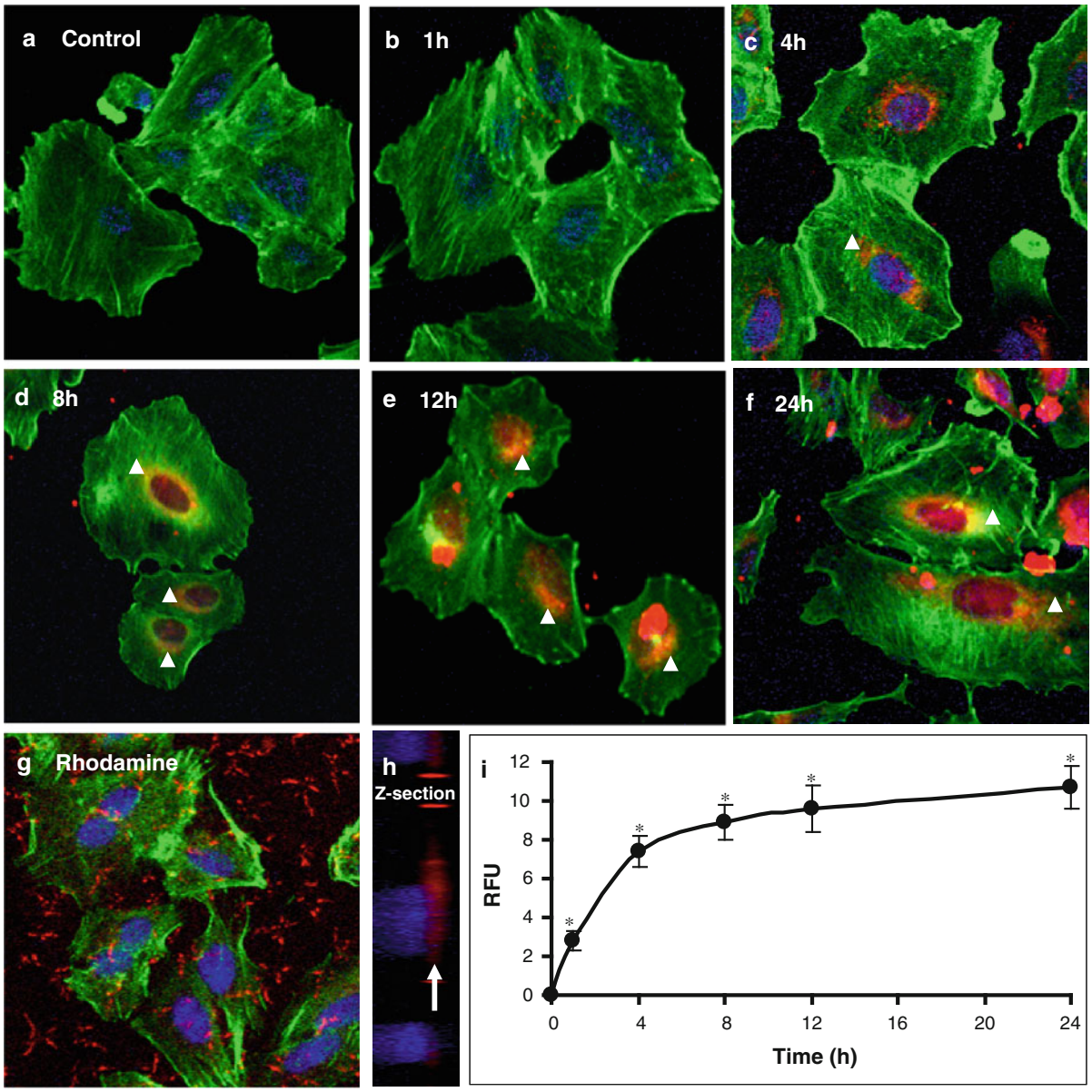

Fig. 2 Cellular uptake of nanoclays by A549 cells. A549 cells growing on 8-well chamber slides (**a**) were incubated with rhodamine (*red*) labeled Cloisite (25 μg/mL) for 1 h (**b**), 4 h (**c**), 8 h (**d**), 12 h (**e**), or 24 h (**f**) and fixed. As a control, cells were treated with rhodamine alone (**g**). Cells were counterstained with Alexa Fluor 488 phalloidin (*green*) and Hoechst (*blue*). Intracellular accumulation of the nanoclays was detected by confocal microscopy and representative images are shown. A z-section of the confocal image (**h**) indicates perinuclear localization of Cloisite nanoclays. Cellular uptake of nanoclays was quantified by a high content analysis approach using an automated microscope IN Cell Analyzer-1000 equipped with Investigator software. The line graph (**i**) is the normalized mean relative fluorescent unit (RFU) values ± SEM of three independent experiments in triplicates from five randomly selected fields per well containing at least 300 cells. $*p < 0.05$ compared to untreated control. *Arrowheads* indicate the unipolar accumulation of labeled (*red*) nanoclays. *Arrow* indicates perinuclear localization of nanoclay particles (*red*). (Color figure online)

agglomerates in A549 cells were observed in a specific manner within the cellular cytoplasm around the nucleus (perinuclear region), but no agglomerates or particles were detectable inside the nucleus (Fig. 2). The z-slicing of labeled Cloisite-treated A549 cells further confirmed intracellular accumulation of

nanoclay particles in the periphery of the nuclear region (red-stained region in Fig. 2h indicated by arrow). The other remarkable feature was the asymmetric unipolar accumulation of nanoclays (arrowheads in Fig. 2). These observations clearly demonstrated that nano-sized clay particles (or agglomerates) are able to enter lung epithelial cells. Quantitation of intracellular Cloisite particles/agglomerates showed time-dependent increase in nanoclay uptake by A549 cells. Significantly high and sustained amount of intracellularly accumulated Cloisite was observed after 1 h of exposure during the time course study of up to 24 h (Fig. 2).

Effect of nanoclays on the viability of A549 cells

To screen the sensitivity of human epithelial cells for nanocalys, A549 cultures were incubated with various concentrations of platelet- or tubular-type nanoclays ranging from 1 to 250 μg/mL for 24 h. The number of viable cells was evaluated using a highly sensitive cell-based high content screening assay utilizing an automated microscope IN Cell Analyzer-1000. None of the nanoclays tested in this study yielded a cytotoxic response at concentrations up to 10 μg/mL, except Delilite LVF which was toxic at 5 μg/mL (Fig. 3). A low but significant decrease in cell viability was observed in A549 cells following treatment with platelet-type nanoclays Bentone MA, ME-100, Cloisite Na^+, Nanomer PGV, or Delilite LVF at concentration 25 μg/mL (Fig. 3a). At higher doses, the ability of cells to grow decreased in a dose-dependent manner following exposure to platelet-type nanoclays with maximal cell population loss occurring at highest concentration (250 μg/mL) as compared to untreated cells (Fig. 3a, b). Overall, Bentone MA and ME-100 were less toxic than other platelet nanoclays at comparable doses (Fig. 3a, b). Interestingly, tubular-type nanoclays Halloysite and Halloysite MP1 showed better compatibility on the viability of A549 cells compared with platelet type. No significant cytotoxic effect was observed when A549 cells were exposed to up to 100 μg/mL concentration of Halloysite or Halloysite MP1 (Fig. 3a, b).

As specific surface area of nanoparticles is an important physical determinant of cytotoxicity, we plotted cell viability data following exposure to 25, 50, or 100 μg/mL concentrations of each nanoclays with their specific surface area (except Nanomer PGV for which specific surface area data not available). An inverse relationship between cell viability and specific surface area of nanoclays is apparent from Fig. 4. Further statistical analysis suggested a high correlation between specific surface area of nanoclays and cell viability following treatment, correlation coefficients being −0.8287 (Fig. 4a), −0.6688 (Fig. 4b), and −0.7185 (Fig. 4c) at concentrations 100, 50, and 25 μg/mL, respectively.

Real-time analysis of cytotoxic effect of nanoclays on A549 cells

In order to evaluate the cytotoxic effect of nanoclays over time, A549 cells were exposed to a high concentration of both nanoclay types (100 μg/mL) and were monitored in real-time for up to 96 h using a whole cell-based electrical impedance sensing technique. Cells were allowed to grow on the electrode to confluence over a period of 20 h before the nanoclays were added. Changes in resistance of the electrode, depending upon various morphological parameters of cells affected by nanoclay treatments, were quantified automatically and plotted as an arbitrary unit Cell Index (Fig. 5). As illustrated in Fig. 5, all the platelet-type nanoclays tested in this study exhibited significant toxicity over time in comparison to tubular nanoclays Halloysite and Halloysite MP1.

Discussion

The issue related to the cytotoxicity of nanomaterials has been a subject of a general concern for nano-inspired research aimed to develop tools for their efficient utilization in biological, medical sciences, and beyond. In this study, we analyzed the cytotoxic effects of two different nanoclay types on human respiratory epithelial cell line A549. Results demonstrate that higher doses of nanoclays cause appreciable cell death in A549 cells, which is of concern if they are to be potentially used for biomedical purposes.

Recently, several publications have advocated the use of in vitro models as efficient nanotoxicity screening tools. As little information is available about potential toxic effects of ever-increasing numbers of nanomaterial, simple and sensitive in vitro toxicity screening platforms are of major importance. In vitro models are rapid, convenient, and cost-

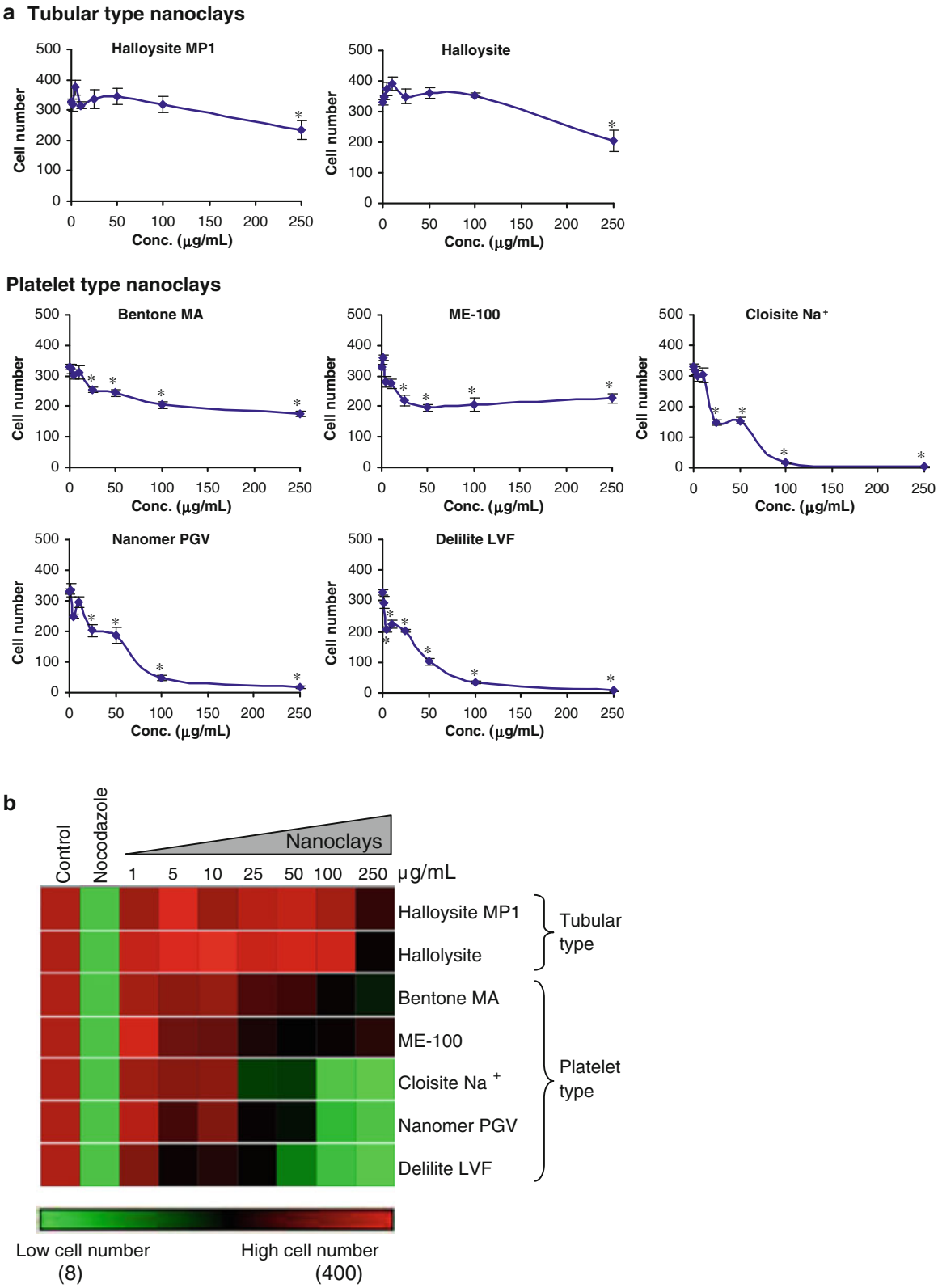
a
Tubular type nanoclays
Halloysite MP1
Halloysite
Platelet type nanoclays
Bentone MA
ME-100
Cloisite Na+
Nanomer PGV
Delilite LVF
Cell number
Conc. (μg/mL)
b
Control
Nocodazole
Nanoclays
1 5 10 25 50 100 250 μg/mL
Halloysite MP1
Hallolysite
Bentone MA
ME-100
Cloisite Na +
Nanomer PGV
Delilite LVF
Tubular type
Platelet type
Low cell number
(8)
High cell number
(400)

◀ **Fig. 3** High content screening and biocompatibility analysis of nanoclays in A549 cells. A549 cells growing on 96-well tissue culture plates were incubated with the indicated nanoclays (1, 5, 10, 25, 50, 100, or 250 μg/mL) for 24 h and fixed. Cells were counterstained with Alexa Fluor 488 phalloidin (*green*) and Hoechst (*blue*). Biocompatibility analysis of the nanoclays was performed using an automated microscope IN Cell Analyzer-1000 equipped with Investigator software by quantifying cell adherence to the plates. **a** Normalized cell numbers ± SEM of three independent experiments in triplicates from five randomly selected fields per well containing at least 300 cells were plated as *line graphs* and presented. $*p < 0.05$ compared to untreated control. **b** A heatmap summarizing the high content screening data was generated and presented. (Color figure online)

effective tools for initial screening of nanomaterial toxicity. In this study, we employed a new approach to in vitro biohazard assessment of nanomaterials incorporating cell-based high content screening and real-time electrical impendence measurements. High content screening operates by automated unbiased image acquisition and analysis. Impedance sensing technique permits environmental control and very closely imitates in vivo physiological conditions. Thus, this multi-modal in vitro approach offers potential advantages for nanotoxicology studies in general.

In order to investigate cellular uptake of nanoclays by A549 cells in this study, we exploited an opportunity to covalently link Cloisite Na^+ with a fluorescent dye rhodamine. Despite the fact that covalent linking of a dye to nanoparticles may alter their characteristics to some extant, it is considered as a good indicative system for cellular uptake analysis. Confocal microscopic examination of cells exposed to rhodamine-labeled Cloisite revealed intracellular presence of nanoclay particles. This observation clearly confirms that nanoclays (or agglomerates thereof) are able to enter lung cells. Previous study has demonstrated endocytosis of various ultrafine particles by A549 cells (Stearns et al. 2001). In this study, Cloisite nanoclays were found to accumulate in a region adjacent to the cell nucleus (perinuclear region), the clustering being polarized in a small niche around the nucleus. The mechanism of this microscopically detectable pattern of interacellular accumulation of nanoclays is not clear. Although it requires more detailed future study to understand this phenomenon, there may be a direct crosstalk between nanoclays and cellular and/or subcellular receptors. The perinuclear region of the cell is comprised of recycling endosomes, and has high lysosomal enzyme activity due to an acidic environment (pH 5.0). This suggests that nanoclays could be accumulated in the perinuclear region of the cell as part of the process of their degradation and/or recycling and subsequent clearance. Our research group has recently demonstrated the possibility of biodegradation of inorganic materials such as single-walled carbon nanotubes by human neutrophils (Kagan et al. 2010). The understanding of the origin of such cell-specific responses may be an important step forward in nanomedicine involving nanoclays. Cloisite particles were not detected within the nuclei confirming that they do not penetrate the nuclear membrane. It is, however, possible, that particles with a size below the resolution of the microscope (therefore undetectable) can pass through the nuclear membrane.

Physicochemical characteristics of nanomaterials such as size, shape, structure, specific surface area,

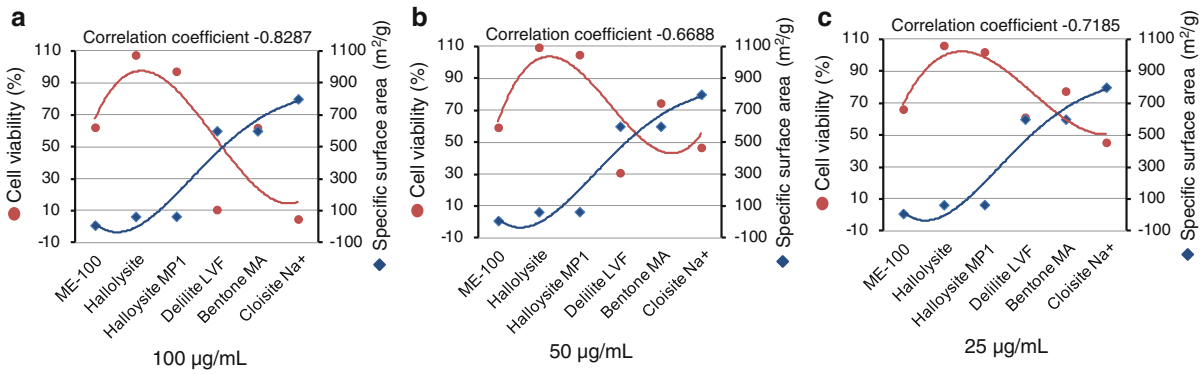

Fig. 4 Cell viability percentage plotted as a function of specific surface area. Percentage (%) A549 cell viability data following treatment with 100 μg/mL (**a**), 50 μg/mL (**b**), and 25 μg/mL (**c**) concentrations of nanoclays were platted as a function of ascending values of their specific surface area. Correlation coefficient values are indicated for each plot

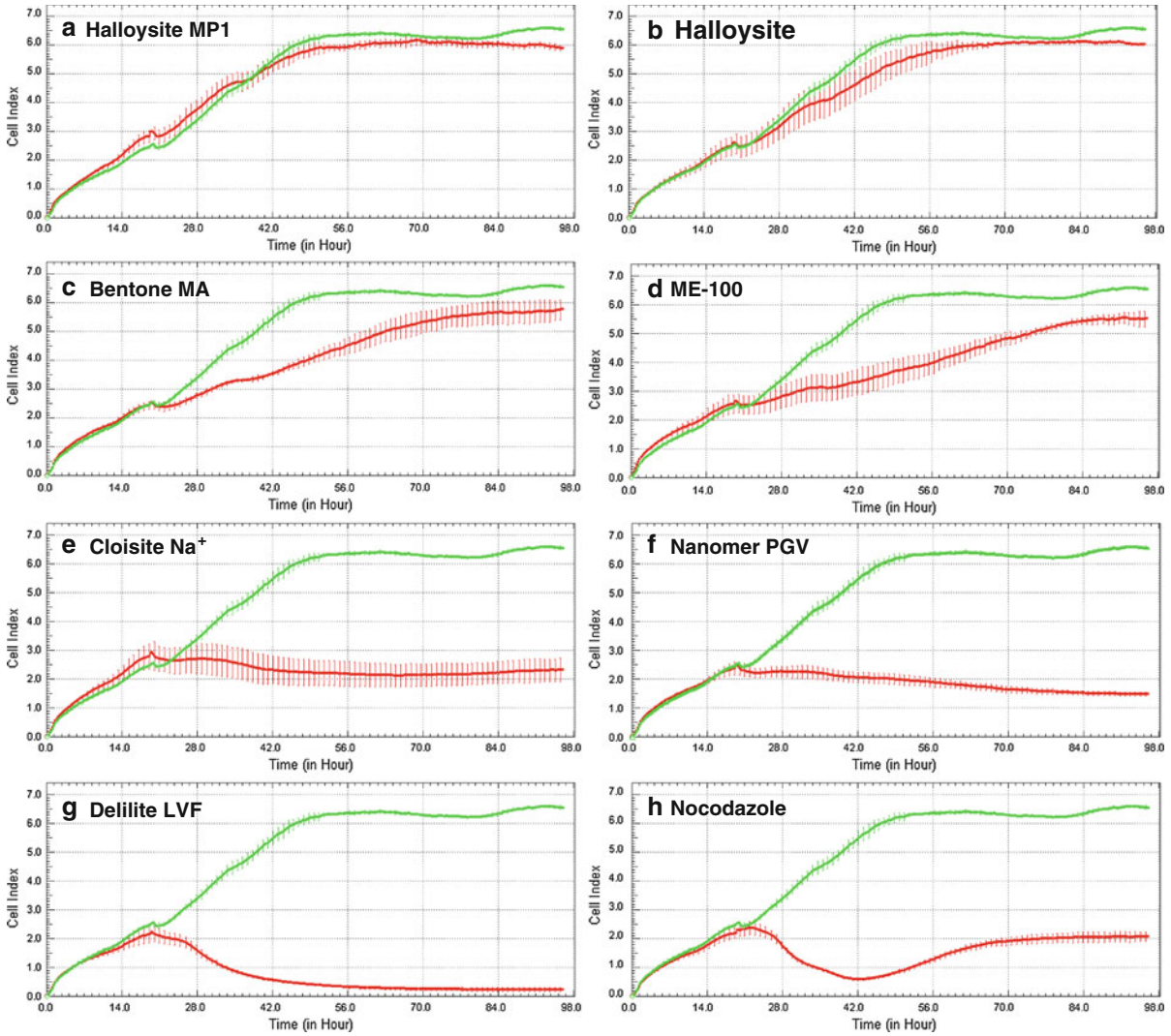

Fig. 5 Real-time biocompatibility analysis of nanoclays on A549 cells by impedance sensing. A549 cells (5×10^3 cells/well) growing on 96-well E-plates for 20 h were treated with the nanoclays (100 μg/mL) in triplicates and incubated for additional 76 h. Names of nanocaly types are indicated on the graphs (**a**–**g**). Cells were treated with Nocodazole (a cytoskeletal disrupting drug) as a control (**h**). Cell growth curves (untreated green vs treated red) were automatically recorded by dynamic monitoring of cell adhesion and spreading process using xCELLigance electrical impedance sensing platform. Data represent cell index ± SEM of three independent experiments performed in triplicates. (Color figure online)

zeta potential, chemical composition, reactive core/shell metals, surface properties, etc., are proposed to be critical determinants of their toxic potential (Nel et al. 2006; Warheit 2008). Depending on these properties, nanoclays can settle, diffuse, and aggregate eventually in the solution. These processes can thus affect the nature of the nanoclays and can also lead to the development of physicochemical stress over the cells. Therefore, we characterized these parameters for all the nanoclays used in this study. The zeta potential data indicated that the nanoclays produced stable dispersions due to presence of charge on their surfaces leading to large repulsive forces between the particles. The presence of charge accumulation on their surfaces could explain the interactions between the nanoclays and the cells but further studies need to be carried out to confirm this.

In this study, we found a high correlation between the specific surface area of nanoclays and cytotoxicity induced by each of them. Previous in vivo studies have

also demonstrated a good correlation between the specific surface area of the particles and the inflammatory response of the exposed animal (Stoeger et al. 2006; Brown et al. 2001). However, some of previous studies failed to demonstrate such a relationship (Warheit et al. 2006; Soto et al. 2007). This discrepancy observed with various nanoparticle in previous studies could be the result of differential penetration, generation of oxidative stress, inflammation, or a combination of several events that result in a particular toxicity mechanism. Of note, primary particle size considerations may sometime be misleading, particularly when considering the aggregation propensity of nanomaterials, particularly in a biological medium containing salts and proteins. Clearly, more studies are needed to have a comprehensive understanding of nanoclay-induced toxicity.

The chemical composition of the particles or their specific geometry appears directly responsible for the decreased cell viability. Here, we demonstrate a noticeable difference in the number of detached and deformed cells as well as the A549 cell viability levels due to platelet-type nanoclays as compared to tubular type. Our results are in consistent with a recently documented report demonstrating cytotoxicity of unmodified and organically modified nanoclays in the human hepatic cell line HepG2 (Lordan et al. 2011). Another study has shown no effect of Cloisite Na^+ on cellular DNA integrity (Sharma et al. 2010). However, the information on how nanoclay particles react with biological systems remains unclear. Additional research is required to evaluate mechanisms of toxicity of nanoclay particles in mammalian cells and evaluate biochemical pathways.

The variable responses of different nanoclays by A549 cells described in this study underscore the need for careful in vitro evaluation of clay nanoparticle effects across a spectrum of relevant cell types, followed by appropriate in vivo studies to provide comprehensive screening datasets regarding the toxicity of nanosize clay particles. These factors are also important considerations for the potential incorporation of nanoclays into novel nanotechnology-based materials. The results from these studies can facilitate future decisions on assessing the potential risk of nanomaterial exposure and health effects.

Acknowledgments The authors would like to acknowledge Enterprise Ireland for financial support under the Grant Number PC/2009/0036 thorough commercialization technology programme. NKV was supported by the SFI funded CRANN-HP collaboration during a part of this study.

References

Ahamed M (2011) Toxic response of nickel nanoparticles in human lung epithelial A549 cells. Toxicol In Vitro 25:930–936

Brown DM, Wilson MR, MacNee W, Stone V, Donaldson K (2001) Size-dependent proinflammatory effects of ultrafine polystyrene particles: a role for surface area and oxidative stress in the enhanced activity of ultrafines. Toxicol Appl Pharmacol 175:191–199

Dong Y, Feng SS (2005) Poly(D,L-lactide-co-glycolide)/montmorillonite nanoparticles for oral delivery of anticancer drugs. Biomaterials 26:6068–6076

Floody MC, Theng BKG, Reyes P, Mora ML (2009) Natural nanoclays: applications and future trends: a Chilean perspective. Clay Min 44:161–176

Kagan VE, Konduru NV, Feng W, Allen BL, Conroy J, Volkov Y, Vlasova II, Belikova NA, Yanamala N, Kapralov A, Tyurina YY, Shi J, Kisin ER, Murray AR, Franks J, Stolz D, Gou P, Seetharaman JK, Fadeel B, Star A, Shvedova AA (2010) Carbon nanotubes degraded by neutrophil myeloperoxidase induce less pulmonary inflammation. Nature Nanotechnol 5:354–359

Lin FH, Lee YH, Jian CH, Wong JM, Shieh MJ, Wang CY (2002) A study of purified montmorillonite intercalated with 5-fluorouracil as drug carrier. Biomaterials 23:1981–1987

Lordan S, Kennedy JE, Higginbotham CL (2011) Cytotoxic effects induced by unmodified and organically modified nanoclays in the human hepatic HepG2 cell line. J Appl Toxicol 31:27–35

Mohamed BM, Verma NK, Prina-Mello A, Williams Y, Davies AM, Bakos G, Tormey L, Edwards C, Hanrahan J, Salvati A, Lynch I, Dawson K, Kelleher D, Volkov Y (2011) Activation of stress-related signalling pathway in human cells upon SiO_2 nanoparticles exposure as an early indicator of cytotoxicity. J Nanobiotechnol 9:29

Napierska D, Thomassen LCJ, Lison D, Martens JA, Hoet PH (2010) The nanosilica hazard: another variable entity. Part Fibre Toxicol 7:39

Nayak PL, Sahoo D (2011) Chitosan-alginate composites blended with cloisite 30B as a novel drug delivery system for anticancer drug paclitaxel. Int J Plast Technol 15:68–81

Nel A, Xia T, Madler L, Li N (2006) Toxic potential of materials at the nanolevel. Science 311:622–627

Oberdorster G, Maynard A, Donaldson K, Castranova V, Fitzpatrick J, Ausman K, Carter J, Karn B, Kreyling W, Lai D, Olin S, Monteiro-Riviere N, Warheit D, Yang H (2005a) Principles for characterizing the potential human health effects from exposure to nanomaterials: elements of a screening strategy. Part Fibre Toxicol 2:8

Oberdorster G, Oberdorster E, Oberdorster J (2005b) Nanotoxicology: an emerging discipline evolving from studies of ultrafine particles. Environ Health Perspect 113:823–839

Powers KW, Brown SC, Krishna VB, Wasdo SC, Moudgil BM, Roberts SM (2006) Research strategies for safety evaluation of nanomaterials. Part VI. Characterization of nanoscale particles for toxicological evaluation. Toxicol Sci 90:296–303

Sharma AK, Schmidt B, Frandsen H, Jacobsen NR, Larsen EH, Binderup ML (2010) Genotoxicity of unmodified and organo-modified montmorillonite. Mutat Res 700:18–25

Soto K, Garza KM, Murr LE (2007) Cytotoxic effects of aggregated nanomaterials. Acta Biomater 3:351–358

Stearns RC, Paulauskis JD, Godleski JJ (2001) Endocytosis of ultrafine particles by A549 cells. Am J Respir Cell Mol Biol 24:108–115

Stoeger T, Reinhard C, Takenaka S, Schroeppel A, Karg E, Ritter B, Heyder J, Schulz H (2006) Instillation of six different ultrafine carbon particles indicates a surface area threshold dose for acute lung inflammation in mice. Environ Health Perspect 114:328–333

Suresh R, Borkar SN, Sawant VA, Shende VS, Dimble SK (2010) Nanoclay drug delivery system. Int J Pharm Sci Nanotechnol 3:901–905

Warheit DB (2008) How meaningful are the results of nanotoxicity studies in the absence of adequate material characterization? Toxicol Sci 101:183–185

Warheit DB, Webb TR, Sayes CM, Colvin VL, Reed KL (2006) Pulmonary instillation studies with nanoscale TiO_2 rods and dots in rats: toxicity is not dependent upon particle size and surface area. Toxicol Sci 91:227–236